Pergamon

Int. J. Solids Structures Vol. 33, No. 29, pp. 4309–4326, 1996
Published by Elsevier Science Ltd
Printed in Great Britain
0020 7683/96 S15.00 + .00

0020–7683(95)00233–2

MATRIX CRACK IMPINGING ON A FRICTIONAL INTERFACE IN UNIDIRECTIONAL BRITTLE MATRIX COMPOSITES

G. P. TANDON
AdTech Systems Research Inc., 1342, North Fairfield Road, Dayton, OH 45432, U.S.A.

and

N. J. PAGANO
WL/MLBM, Wright Patterson AFB, Dayton, OH 45433, U.S.A.

(*Received* 31 *May* 1995; *in revised form* 22 *September* 1995)

Abstract—The objective of this work is to study the effect of a frictional interface on the extent of interfacial debonding and internal stress distribution within a unidirectional ceramic matrix composite under thermo-mechanical loading. The configuration considered is a concentric cylinder with an annular crack in the axial plane of the matrix while the fiber-matrix interface is made to obey the Coulomb friction law. The present approach of employing a variational model is shown to satisfy all boundary and inequality conditions in the slip and stick regions and at the slip-stick transition point. The results are also shown to be in very good agreement with a numerical elasticity solution for points away from the matrix crack tip while some of the peculiarities near the crack tip associated with the numerical solution are identified. Published by Elsevier Science Ltd.

INTRODUCTION

In this work we are interested in a class of composites commonly referred to as brittle matrix composites (BMC) that are characterized by continuous fibers with an elastic matrix that possesses stiffness which may be comparable to that of the fiber. A prominent feature of BMC geometry is the presence of imperfect bonding between the various constituent materials, such as the fiber-matrix interface. In this class of composites, cracks will first develop in the matrix under tensile loading in the axial direction due to its lower failure strain. When a matrix crack approaches the fiber-matrix interface, the interface may open or slip, thereby blunting the crack by slowing and/or arresting its propagation. Although the blunting of the crack increases the fracture toughness of the composite (Budiansky *et al.*, 1986), the damage in the interface reduces the axial compressive and transverse strength of the composite and is also one of the major causes of stiffness reduction in the fiber direction (Steif, 1984).

Theories for the strength and toughness of fiber-reinforced composites have, for the most part, been based on rather simple assumptions regarding the way in which load is transferred between the fiber and the matrix. These theories (Kelly, 1970; Aveston *et al.*, 1971) typically assume that a constant shear stress acts at the fiber-matrix interface. This shear stress is often interpreted as the flow stress of the matrix or as the friction stress at the interface. According to Dollar and Steif (1988), using a constant shear stress model for a fiber-matrix interface which is actually governed by Coulomb friction may lead to substantially inaccurate results. Dollar and Steif (1988) have shown that the constant shear stress approximation overestimates the amount and extent of slip when the fiber is subjected to compression, while underestimating these quantities when the fiber is subjected to tension. On the other hand, one should also realize an intrinsic difficulty of models that represent fiber and matrix as layers. Such models provide inaccurate representation of geometric details such as the ratio of fiber spacing to fiber diameter which can differ drastically from

that in a composite having the same volume fraction of fibers arranged in a hexagonal pattern. This distortion is especially magnified at low values of fiber volume fraction. There is substantially less distortion of these details in the concentric cylinder model utilized in this work, although the idealization of an initial annular crack in this case carries its own question of credibility.

Axisymmetric three-dimensional failure mechanics models, which satisfy all equations of elasticity as well as assume an imperfect interface, include the works of Wijeyewickrema and Keer (1993), Kaw and Pagano (1993), Meda *et al.* (1993), Selvadurai (1994) and Kaw *et al.* (1995). The interface in the work of Wijeyewickrema and Keer (1993) included a slip zone and was assumed to have a constant shear stress equal to the shear strength of the interface. Kaw and Pagano (1993) approximated the imperfect interface by distributed shear springs of constant stiffness. The fiber micro-indentation push-in test was studied by Meda *et al.* (1993) for the case of a Coulomb friction law by considering a single fiber embedded in a half-space. Selvadurai (1994) used the boundary element technique to examine the self-similar extension of a matrix crack in the presence of Coulomb friction at the interface. The assumptions of dilute fiber volume fraction and a through annular crack in the work of Schwietert and Steif (1991) were relaxed by Kaw *et al.* (1995). Further, Schwietert and Steif (1991) simulated the residual compression at the interface (for systems in which $\alpha_m > \alpha_f$) by applying a remote stress acting to press the regions together. This idealization, however, fails to recognize the spatial distribution of the residual stress field, especially where the singular nature of the radial stress at the free surface actually leads to a sign reversal in σ_r (Pagano, 1991). Kaw *et al.* (1995) directly accounted for the processing induced residual stresses in their work, where, using a related boundary element method, the system of equations was reduced to coupled integral equations which were then solved numerically.

The objective of this work is to accurately examine the stress and displacement fields in the vicinity of matrix cracks approaching a frictionally constrained interface. In this study a modified version of the variational model (Pagano, 1991) of an axisymmetric concentric cylinder has been employed. After deriving the sliding interface boundary conditions, we will specifically examine the effect of the friction coefficient, temperature change and remote uniform axial displacement on the extent of interfacial debonding and internal stress distribution within a unidirectional ceramic matrix composite under thermo-mechanical loading. We will compare our results with the solution of Kaw *et al.* (1995) for an identical geometry and loading. We should note that our main purpose here is to qualify our model for use to solve problems which involve a frictional interface. As we shall see later (see concluding remarks), the example problem posed is unlikely to be realized in practice, even under very idealized conditions. This work then is viewed as a prerequisite to attacking the more realistic problems. It goes without saying that more approximate treatments, such as shear-lag models, also suffer this deficiency.

PROBLEM DEFINITION

The medium considered here consists of a solid cylindrical body (fiber) which is surrounded by a concentric hollow cylinder (matrix) as shown in Fig. 1. This concentric cylinder configuration can be viewed as an approximation for the representative volume element of a unidirectional composite reinforced by a hexagonal array of fibers. Cylindrical coordinates r, z are introduced as shown in Fig. 1 and each material is assumed to be elastically transversely-isotropic with respect to the z axis.

Let the fiber radius and the matrix outer radius be denoted by a and d, respectively. The composite cylinder is subjected to a monotonically increasing axial displacement w_0 on the ends plus a constant temperature change ΔT. Under tensile loading in the axial direction, cracks will first develop in the matrix region due to its lower failure strain than that of the fiber. An annular crack of length '$c-b$' ($a \leqslant b < c \leqslant d$) is therefore introduced in the matrix in the $z = 0$ plane, at a distance of '$b-a$' from the interface. When the matrix crack reaches the fiber-matrix interface, the interface may open or slip. This opening/slipping of the interface blunts the crack, and thereby slows and/or arrests its propagation. For analysis

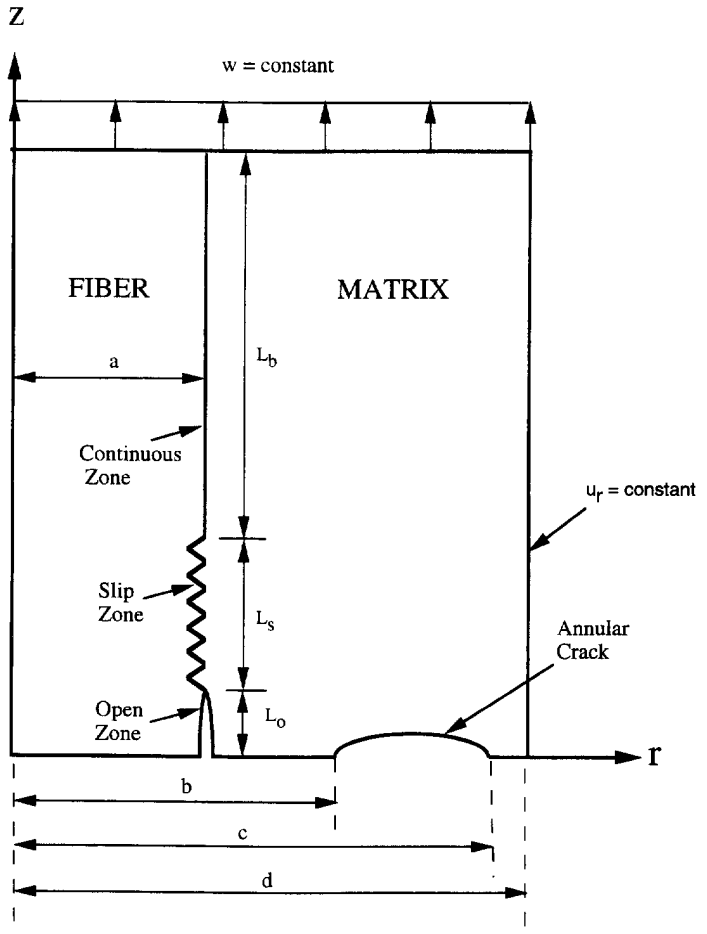

Fig. 1. Schematic of a representative volume element with a frictional interface and annular matrix crack.

purposes, the interface between the fiber and matrix may have open, slip and continuous zones, and their lengths are denoted by L_o, L_s and L_b, respectively, as shown in Fig. 1.

BOUNDARY CONDITIONS

Interface conditions

The traction continuity conditions at the interface between the fiber and matrix $(0 \leqslant |z| \leqslant (L_o+L_s+L_b))$ at $r = a$ are given by

$$\sigma_{rr}^{f}(a,z) = \sigma_{rr}^{m}(a,z), \quad \sigma_{rz}^{f}(a,z) = \sigma_{rz}^{m}(a,z) \tag{1}$$

where the superscripts f and m refer the stated quantity to the fiber and matrix, respectively. In addition, in each one of the regions, namely, the open, slip and continuous regions, the following conditions need to be satisfied.

Open zone $(0 \leqslant |z| \leqslant L_o)$: the crack surfaces are traction free as given by

$$\sigma_{rr}^{f}(a,z) = 0, \quad \sigma_{rz}^{f}(a,z) = 0 \tag{2}$$

and are constrained by the crack opening condition

$$u^m(a,z) - u^f(a,z) > 0 \tag{3}$$

where the r, z components of displacement are designated as u, w, respectively.

Slip zone ($L_o \leqslant |z| \leqslant (L_o + L_s)$): for this work, the interface between the fiber and matrix is made to follow the Coulomb friction law and the friction coefficient μ is assumed to be constant in the slip zone. The shear stress in the slip region is related to the radial stress through

$$\sigma^f_{rz}(a,z) = \pm \mu \sigma^f_{rr}(a,z) \tag{4}$$

where the sign to be used is determined by the consideration that the shear stress opposes the relative slip (Δw) at the interface. In addition, the radial stress in the slip region is compressive, i.e.,

$$\sigma^f_{rr}(a,z) < 0 \tag{5}$$

while normal contact is maintained

$$u^f(a,z) = u^m(a,z). \tag{6}$$

Continuous zone ($(L_o + L_s) \leqslant |z| \leqslant (L_o + L_s + L_b)$): the radial and axial displacements are continuous at the interface

$$u^f(a,z) = u^m(a,z), \quad w^f(a,z) = w^m(a,z) \tag{7}$$

In the present model, the continuous zone is not constrained to be a "stick" region, i.e., the radial stress may be tensile (so long as it does not exceed the interfacial normal strength value). For frictionally constrained interfaces (i.e., interfaces with zero intrinsic normal strength) the radial stress is constrained to be compressive

$$\sigma^f_{rr}(a,z) < 0 \tag{8}$$

while the absolute value of the shear stress is such that it does not allow slip

$$|\sigma^f_{rz}(a,z)| < \mu |\sigma^f_{rr}(a,z)| \tag{9}$$

Surface conditions

At points on the surface ($r = d$), we can impose two sets of elasticity boundary conditions

$$\sigma^m_{rz}(d,z) = \sigma^m_{rr}(d,z) = 0 \tag{10}$$

or

$$u^m(d,z) = u^T(d,z) + u^M(d,z)$$
$$\sigma^m_{rz}(d,z) = 0 \tag{11}$$

as bounds since eqns (10) minimize and eqns (11) maximize the constraint within the class of problems having zero shear stress on the boundary (the latter requirement is motivated by the concentric cylinder simulation of the hexagonal array). In these equations $u^T(d,z)$

and $u^M(d,z)$ are the radial displacements in the uncracked composite due to a temperature change, ΔT, and remote axial displacement w_0, respectively. The stress and displacement fields for a perfectly bonded composite cylinder subjected to a uniform remote axial strain and thermal loading are given by Chawla (1987) and Hseuh and Becher (1988, 1989), respectively, and are conveniently summarized in the appendix of Kaw *et al.* (1995). At points on the surface, $r = d$, well removed from the crack plane, the two conditions (10) and (11) are equivalent. In this work, we will use eqns (11) since these lead to zero slope of the crack surface, $\partial w^m/\partial r$, at $(d,0)$ for the edge crack problem ($c = d$) and avoid the cusp which would result from the application of eqns (10).

End condition

The elasticity boundary conditions to be prescribed at the crack plane $z = 0$, are given by

$$\begin{aligned}
&\sigma_{rz}^f(r,0) = 0 \quad r \leqslant a \\
&\sigma_{rz}^m(r,0) = 0 \quad a \leqslant r \leqslant d \\
&w^f(r,0) = 0 \quad r \leqslant a \\
&w^m(r,0) = 0 \quad a \leqslant r \leqslant b, \quad c \leqslant r \leqslant d \\
&\sigma_{zz}^m(r,0) = 0 \quad b \leqslant r \leqslant c
\end{aligned} \tag{12}$$

constrained by the opening of the transverse crack

$$w^m(r,0) \geqslant 0, \quad b \leqslant r \leqslant c \tag{13}$$

VARIATIONAL MODEL

The solution for the stated problem is obtained by employing a modified version of the variational model (Pagano, 1991) of an axisymmetric concentric cylinder which contains damaged regions in the form of annular or penny-shaped cracks in the constituents and/or debonds between them. The model is generated by subdividing the body into regions consisting of a core and a number of shells of constant thickness and length and satisfying the Reissner variational equation with an assumed stress field in each region. That is, we set

$$\delta J = 0 \tag{14}$$

where

$$J = \int_V F \,\mathrm{d}v - \int_{S'} \tilde{T}_i U_i \,\mathrm{d}S \tag{15}$$

and

$$F = \frac{1}{2}\tau_{ij}(U_{i,j} + U_{j,i}) - W(\tau_{ij}, e_{ij}) \tag{16}$$

In these equations, W is the complementary energy, τ_{ij} and U_i are the stress and displacement components, respectively, in Cartesian coordinates, e_{ij} are the mathematical free expansional or non-mechanical strains, V is the volume enclosed by S, S' is the part of S on which one or more traction components are prescribed and $\tilde{T}_i$ are the Cartesian components

of the prescribed tractions. Further, a comma followed by a subscript(s) implies differentiation with respect to the appropriate coordinate(s) and the summation convention is understood. Throughout this work, we also define the tilde functions as follows:

$$\tilde{f}(x) = \begin{cases} f(x) & \text{if } f \text{ is prescribed at } x \\ 0 & \text{otherwise} \end{cases}$$

Reissner (1950) has shown that the governing equations of elasticity can be obtained as a consequence of the variational equation provided both stresses and displacements are subject to variation in the application of (14). The stress field is assumed such that σ_{zz} and $\sigma_{\theta\theta}$ are linear in r within each region, while the forms of σ_{rr} and σ_{rz} are chosen to satisfy the axisymmetric equilibrium equations of linear elasticity. Letting

$$\sigma_1 = \sigma_{zz}, \quad \sigma_2 = \sigma_{\theta\theta}, \quad \sigma_3 = \sigma_{rr}, \quad \sigma_5 = \sigma_{rz} \tag{17}$$

(and the analogous relation for the engineering strain components ε_i $(i = 1,2,3,5)$ and hygrothermal free expansional strain components e_i $(i = 1,2,3)$), we arrive at the relations in the region $r_1 \leqslant |r| \leqslant r_2$

$$\sigma_i = p_{iJ} f^{(i)}_J \quad (i = 1,2,3,5; J = 1,2,\ldots 5) \tag{18}$$

where $f^{(i)}_J$ are known shape functions of r defined such that

$$p_{i\alpha}(z) = \sigma_i(r_\alpha, z) \quad (i = 1,2,3,5; \alpha = 1,2) \tag{19}$$

and the inner and outer radii of the region are denoted by r_1 and r_2, respectively. In order to maintain consistency with our postulated stress field, we further assume that eqns (18) hold on the boundaries, as well as within the medium itself. The remaining dependent variables follow directly from the mathematics without further assumptions. They are the weighted displacements

$$(\tilde{u}, u^*, \hat{u}, \bar{\tilde{u}}) = \int_{r_1}^{r_2} u(1, r, r^2, r^3)\, \mathrm{d}r \tag{20}$$

and

$$(w^*, \hat{w}) = \int_{r_1}^{r_2} w(r, r^2)\, \mathrm{d}r \tag{21}$$

The interfacial displacements u_α, w_α $(\alpha = 1,2)$, or displacements on the radial boundaries $r = r_1, r_2$, only enter the formulation if they are prescribed or if we have relative slip at the interface.

For simplicity, let us assume that the medium consists of a single section composed of a cylindrical core $(k = 0)$ surrounded by N concentric hollow cylinders and is defined by end planes $z = z_1, z_2$. Now, according to (14),

$$\delta J = \sum_{k=0}^{N} \delta J_k = 0 \tag{22}$$

for the entire medium. Substituting eqns (16)–(21) into (15) and performing the integration with respect to r after taking the first variation and then into (22), we arrive at

$$\int_{z_1}^{z_2} [(\chi_{32}+r_2u_2)\delta p_{32}+(\chi_{52}+r_2w_2)\delta p_{52}+(p_{32}-\tilde{p}_{32})r_2\delta u_2+(p_{52}-\tilde{p}_{52})r_2\delta w_2]^0\,\mathrm{d}z$$

$$+\{[(H_3-\tilde{H}_3)\delta\hat{u}+(H_4-\tilde{H}_4)\delta\bar{\bar{u}}+(H_7-\tilde{H}_7)\delta w^*+(H_8-\tilde{H}_8)\delta\hat{w}]^0\}_{z=z_1}^{z=z_2}$$

$$+\sum_{k=1}^{N}\int_{z_1}^{z_2}[(\chi_{31}-r_1u_1)\delta p_{31}+(\chi_{51}-r_1w_1)\delta p_{51}+(\chi_{32}+r_2u_2)\delta p_{32}+(\chi_{52}+r_2w_2)\delta p_{52}$$

$$-(p_{31}-\tilde{p}_{31})r_1\delta u_1-(p_{51}-\tilde{p}_{51})r_1\delta w_1+(p_{32}-\tilde{p}_{32})r_2\delta u_2+(p_{52}-\tilde{p}_{52})r_2\delta w_2]^k\,\mathrm{d}z$$

$$+\{[(H_1-\tilde{H}_1)\delta\bar{u}+(H_3-\tilde{H}_3)\delta\hat{u}+(H_4-\tilde{H}_4)\delta\bar{\bar{u}}+(H_7-\tilde{H}_7)\delta w^*$$

$$+(H_8-\tilde{H}_8)\delta\hat{w}]^k\}_{z=z_1}^{z=z_2}=0 \quad (23)$$

where the superscript k attached to a bracket or parenthesis signifies that all the enclosed functions are to be evaluated at the given value of k and

$$\chi_{iJ}=\eta_{iJ}-E_{iJ}-s_{ijKJ}p_{jK} \quad (i,j=1,2,3,5;J,K=1,2,\ldots 5) \quad (24)$$

with

$$E_{iJ}=\int_{r_1}^{r_2} e_i f_J^{(j)} r\,\mathrm{d}r \quad (i,j=1,2,3,5;J,K=1,2,\ldots 5) \quad (25)$$

and

$$s_{ijKJ}=\int_{r_1}^{r_2} S_{ij} f_K^{(j)} f_J^{(j)} r\,\mathrm{d}r \quad (i,j=1,2,3,5;J,K=1,2,\ldots 5) \quad (26)$$

where S_{ij} is the elastic compliance matrix and the components of η_{iJ} are defined in the Appendix. Also, the following definitions have been employed in (23) for the case where $r_1 \neq 0$

$$H_1=p_{53}$$

$$H_3=\frac{r_2^2p_{51}-r_1^2p_{52}}{r_1r_2(r_2-r_1)}-\frac{(r_1^2+r_1r_2+r_2^2)p_{53}}{r_1^2r_2^2}$$

$$H_4=\frac{r_1p_{52}-r_2p_{51}}{r_1r_2(r_2-r_1)}+\frac{(r_1+r_2)p_{53}}{r_1^2r_2^2} \quad (27)$$

while, if $r_1=0$, instead of (27), we have

$$H_1=0, \quad H_3=\frac{p_{52}}{r_2}-r_2p_{53}, \quad H_4=p_{53} \quad (28)$$

and

$$H_7=\frac{r_2p_{11}-r_1p_{12}}{r_2-r_1}$$

$$H_8=\frac{p_{12}-p_{11}}{r_2-r_1} \quad (29)$$

hold for any value of r_1. Further, since the variations of the weighted displacements, $\delta\bar{u}_k \ldots \delta\hat{w}_k$, are all arbitrary in the region, $z_1 < z < z_2$, the coefficients of these terms have

been set equal to zero in (23). These lead to the so called equilibrium equations.† Similarly, aside from $\delta p^k_{31}, \delta p^k_{32}, \delta p^k_{51}, \delta p^k_{52}$, which may enter the boundary conditions and/or interface conditions, the coefficients of the remaining δp^k_{ij} have been set equal to zero in (23) since the variations are arbitrary. These lead to the so called constitutive relations.†

Interface conditions

We will next examine the boundary condition equations derived from the variational principle. At this point we should recall that p_{3i} and p_{5i} $(i = 1,2)$ are simply equal to the radial and shear stress, respectively, at $r = r_i$ as shown by eqn (18), while u_i and w_i are the radial and axial displacement components, respectively, at $r = r_i$. Thus these functions may or may not be independent. In the discussion which follows let k denote the interface between the fiber and matrix.

Open zone. At a point on an interface $r^k_2 = r^{k+1}_1$ $(0 \leqslant k \leqslant N-1)$, we may prescribe traction components. Using (1) and (2), review of eqn (23) indicates that the following options are appropriate

$$p^k_{32} = \tilde{p}^k_{32} = 0, \quad p^k_{52} = \tilde{p}^k_{52} = 0 \tag{30}$$

as well as

$$p^{k+1}_{31} = \tilde{p}^{k+1}_{31} = 0, \quad p^{k+1}_{51} = \tilde{p}^{k+1}_{51} = 0 \tag{31}$$

Slip zone. At a point on an interface $r^k_2 = r^{k+1}_1$ $(0 \leqslant k \leqslant N-1)$ where traction continuity is prescribed (eqn 1), we must have

$$p^k_{32} = p^{k+1}_{31} = p(\text{say}) \tag{32}$$

$$p^k_{52} = p^{k+1}_{51} = \tau(\text{say}) \tag{33}$$

while the conditions of frictional slippage (eqn 4) and normal contact (eqn 6) require

$$u^k_2 = u^{k+1}_1 \tag{34}$$

and

$$p^k_{52} = \pm \mu p^k_{32} \tag{35}$$

where the sign to be used is determined by the consideration that the shear stress should oppose the relative slip (Δw) at the interface. Substituting (32)–(35) and the first variation of these equations into (23), we find that we must set

$$\chi^k_{32} + \chi^{k+1}_{31} \pm \mu(\chi^k_{52} + \chi^{k+1}_{51} + r^k_2 w^k_2 - r^{k+1}_1 w^{k+1}_1) = 0 \tag{36}$$

and prescribe $(w^k_2 - w^{k-1}_1)$ in the slip region, in order for the variation to vanish. However, it is not realistic to impose the relative slip $(w^k_2 - w^{k+1}_1)$ as a boundary condition. To avoid this problem, we propose a modification to the formulation as follows. Use of (32) and (34) in conjunction with (23) without invoking (35) gives

$$\chi^k_{32} + \chi^{k+1}_{31} = 0 \tag{37}$$

We shall use eqns (32), (33), (35) and (37) in the slip region and employ eqn (36) to

†For details see Pagano (1991).

calculate the jump in axial displacement at the slipping boundary as even in 3-D elasticity theory, eqn (14) does not vanish when friction is included.

Continuous zone. At a point on an interface $r_2^k = r_1^{k+1}$ $(0 \leqslant k \leqslant N-1)$ where continuity is prescribed, we must have

$$u_2^k = u_1^{k+1}, \quad w_2^k = w_1^{k+1} \tag{38}$$

and

$$p_{32}^k = p_{31}^{k-1}, \quad p_{52}^k = p_{51}^{k+1} \tag{39}$$

using (1) and (7). Substituting (38), (39) and the first variation of these equations into (23), we get

$$\chi_{32}^k + \chi_{31}^{k+1} = 0, \quad \chi_{52}^k + \chi_{51}^{k+1} = 0 \tag{40}$$

and the interfacial displacements u_i and w_i $(i = 1, 2)$ at this point are eliminated from the equations. Consequently, the proper relations governing interfacial continuity at a point are (39) and (40).

Surface conditions

We see that eqn (23) also contains two terms corresponding to the outer annulus $k = N$. Using (11) and (23), we obtain

$$\chi_{32}^N = -r_2^N \tilde{u}_2^N = -r_2^N \tilde{u}(d,z) \tag{41}$$

and

$$p_{52}^N = \tilde{p}_{52}^N = 0 \tag{42}$$

End conditions

Finally, using (12) and (23), the boundary conditions to be prescribed on the crack plane $z = 0$ can be expressed as follows

$$\left.\begin{aligned} H_1 &= \tilde{H}_1 = 0 \\ H_3 &= \tilde{H}_3 = 0 \\ H_4 &= \tilde{H}_4 = 0 \end{aligned}\right\} \quad r \leqslant d \tag{43}$$

$$\left.\begin{aligned} H_7 &= \tilde{H}_7 = 0 \\ H_8 &= \tilde{H}_8 = 0 \end{aligned}\right\} \quad b \leqslant r \leqslant c \tag{44}$$

$$w^* = \hat{w} = 0 \quad r \leqslant b, \quad c \leqslant r \leqslant d \tag{45}$$

which completes the boundary value problem formulation with the present model. We should mention that while the analysis was presented for a single section, it can be very easily extended to include multiple sections. In that case, the summation in (22) is carried over all sections under consideration.

General solution

Our system consists of $18N+16$ equations for a like number of unknowns which are $p_{11}, p_{12}, p_{21}, p_{22}, p_{31}, p_{32}, p_{33}, p_{34}, p_{35}, p_{51}, p_{52}, p_{53}, \hat{u}, \bar{u}, \bar{\bar{u}}, u^*, \hat{w}, w^*$ within each annulus; and

$p_{11}, p_{12}, p_{21}, p_{22}, p_{31}, p_{32}, p_{33}, p_{34}, p_{52}, p_{53}, \hat{u}, \bar{u}, \bar{\bar{u}}, u^*, \hat{w}, w^*$ in the core, while $5N+4$ boundary conditions are required at each end $z = z_1, z_2$. The field equations within each material, generated by the variational equation, consist of a system of first order ordinary differential equations and algebraic equations of the form

$$[L_1]\vec{x}' + [L_0]\vec{x} = \vec{y}$$

where

- $[L_1]$ contains the coefficients of the derivative terms,
- $[L_0]$ contains the coefficients of the algebriac terms,
- $\vec{y}$ contains the terms dependent on the hygrothermal strains and applied displacements, and
- $\vec{x}$ contains the unknown stress and displacement functions

The general form of the solution for any of the dependent variables $P(z)$ is therefore expressed by

$$P(z) = \sum_i A_i e^{\lambda_i z} + P_p(z) \tag{46}$$

within each constituent where A_i are constants, λ_i are eigenvalues of a determinant, and $P_p(z)$ is a particular solution, which in the present case is a simple polynomial. Further details of the solution procedure including the method for determining the higher order eigenvector and higher order particular solution are discussed by Brown (1992). The number of regions, in particular in the r direction, can be increased in order to improve solution accuracy. The regions are selected such that the thermoelastic properties are constant and the boundary conditions do not change character on any of the bounding surfaces within each region.

EXAMPLE PROBLEM

Our aim is to study the effect of material and geometrical parameters on the extent of interfacial debonding under thermo-mechanical loading of a unidirectional ceramic matrix composite. We will specifically examine the effect of the friction coefficient and temperature change under remote uniform axial displacement on the internal stress distribution. We will compare our results with the solution of Kaw *et al.* (1995) for an identical geometry and loading. Only cases with slip and no open zone were considered in their study, with the edge crack touching the slipping interface, i.e., $a = b$ and $c = d$ (see Fig. 1) which results in a fully cracked matrix. A sufficient condition to ensure no opening occurs is that the stress normal to the interface is compressive over the entire interface; for the cases studied this has been verified *a posteriori*. The absence of any singularities for the stated problem for relevant values of elastic moduli and friction coefficient for ceramic matrix composites is discussed by Schwiertert and Steif (1991), although, as we have discussed earlier (Pagano, 1991), no singularities appear in the present model under our solution technique.

The material properties used in the calculations corresponding to a SiC (silicon carbide) fiber and CAS (calcium aluminosilicate) glass matrix are as follows:

Material	*E (GPa)*	*v*	*α (μm/m/°C)*
SiC	207.0	0.25	3.5
CAS	98.0	0.25	6.5

The fiber volume fraction was set to equal to 0.4 while ΔT was estimated to be $-1000°C$ to calculate the processing induced residual stresses. In all problems studied, the length of the continuous zone normalized by the fiber radius was set equal to 120, while the normalized slip length was a parameter (varied from 1 to 7). The resulting ratio of continuous to slip region is assumed to simulate an infinite continuous region. In general, the z-dependence

of the solution is expressed in closed form. Thus, no further discretization was needed in the z-direction in the two regions considered, i.e., the continuous and slip zones (this would only be necessary to avoid overflow/underflow problems). The results of the model, as mentioned earlier, however demonstrate dependence on the thickness of the subregions taken to represent the domain. In the present case, results were obtained with ten subregions, one core and nine shells, with the interfaces chosen at $r = 0.7\ a$, $0.85\ a$, $0.92\ a$, $0.97\ a$, a, $1.03\ a$, $1.12\ a$, $1.25\ a$ and $1.4\ a$. Some of the details of subregion optimization have been discussed earlier (Pagano, 1991; Pagano and Brown, 1993); however, this still remains dependent on a trial and error approach. We have not conducted any further convergence studies, but based on our past experience, we feel confident with the numerical scheme employed in this work. The calculations were done on a HP 9000 computer employing quad precision.

In general, slip length L_s, is dependent on several parameters such as the externally applied remote displacement w_0, friction coefficient μ, and temperature change ΔT, besides the thermoelastic properties of the constituents. Several researchers have used a criterion which supplements the aforementioned boundary conditions to estimate the length of the slip zone. These include, amongst the many employed, using (i) smoothness of shear stress (Kaw *et al*, 1995), and (ii) continuity of interfacial stresses and displacement gradients (Schwietert and Steif, 1991) at the stick-slip transition, or (iii) setting the total stress intensity factor equal to zero (Wang *et al.*, 1991; Dollar and Steif, 1989) at the matrix crack tip (because of absence of singularity at that point for the problem under consideration). For this study, we assume a constant value of the length of the slip zone and change the input remote displacement iteratively (while keeping everything else constant) so that all our boundary, inequality and sign conditions are satisfied. The resulting solution is seen to satisfy the continuity of axial, shear and radial stresses corresponding to a smooth transition from a slip to a stick zone in both fiber and matrix.

In subsequent plots, the results from the present analysis are indicated by lines (solid and dotted) whereas symbols will represent the solution taken from the work of Kaw *et al.* (1995).

In Fig. 2, we have plotted the normalized slip length L_s/a as a function of the negative of the ratio of remote matrix axial stress to remote interfacial radial stress. This is because any combination of temperature change, remote axial displacement and linear coefficients of thermal expansion of the fiber and matrix which result in the same stress ratio will result

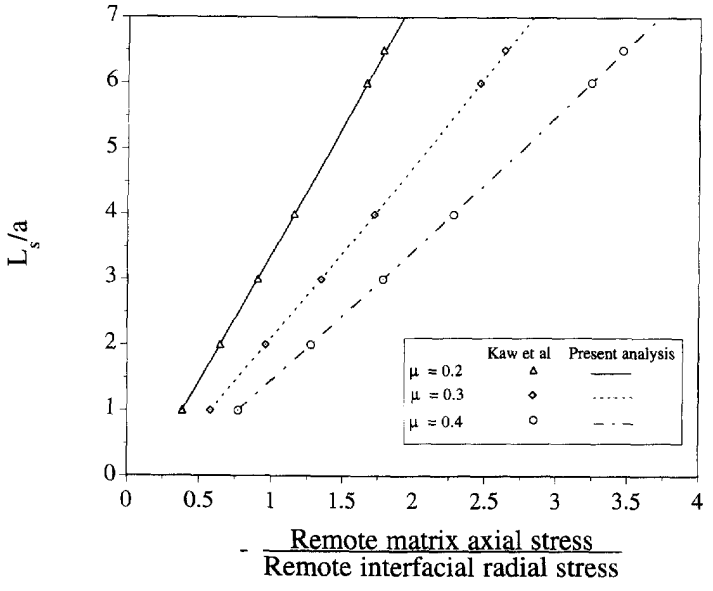

Fig. 2. Variation of normalized slip length as a function of the negative of the stress ratio for constant coefficient of friction.

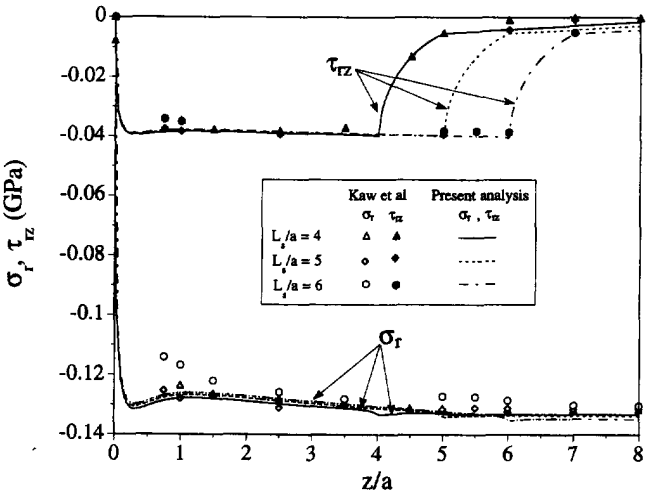

Fig. 3. Interfacial radial and shear stresses as a function of normalized axial location for constant slip lengths.

in the same slip length. Unlike the comparison with results of Gu and Mangonon† (1992), (see Fig. 4 in Kaw *et al.*, 1995), we observe very good agreement between the present analysis and the numerical solution of Kaw *et al.* (1995) for all choices of coefficient of friction and all values of slip lengths. The slip length increases monotonically with an increase in stress ratio and decreases with an increase in coefficient of friction.

Next, we compare the stress distribution at the fiber-matrix interface as a function of normalized axial location, z/a, from the matrix crack plane. For the remainder of this study, we will set the friction coefficient to be 0.3. In Fig. 3, we have shown the distribution of the radial and shear stress at the interface and compared our solution with the results of Kaw *et al.* (1995). Unlike the numerical solution, where eqn (4) is satisfied only at a discrete number of collocation points, the present analysis satisfies the Coulomb friction law at all points within the slip region, including the point $z/a = 0$ which is on the crack plane. In the numerical scheme employed by Kaw *et al.* (1995), the first collocation point‡ is located away from the crack plane. The calculated value of the radial stress is therefore close but not equal to zero at the matrix crack tip (the shear stress is equal to zero at the matrix crack plane) since the Coulomb friction law is not being satisfied there. As seen in Fig. 3, the radial stress rapidly approaches the remote radial stress at the interface whereas, the shear stress decays rapidly to zero at the end of the slip zone. Both the interfacial radial stress and maximum shear stress are seen to be insensitive to increasing slip length. Within the slip zone, the shear stress is seen to increase from zero at the free surface to a large negative value (approx. 40 MPa) within a small region adjacent to the surface. For the various slip lengths investigated this boundary layer effect is seen to occur within one-half of fiber radius irrespective of the value of the slip length, as shown in Fig. 4. Having attained the maximum, the shear stress then remains fairly constant within the slip region. Various approximate models available in the literature, which assume a constant value of shear stress in the slip region, therefore neglect the boundary layer effect observed in this study. Also, one should note that a constant shear stress assumption gives logarithmically singular fiber axial stresses at the crack tip (Wijeyewickrema and Keer, 1993), while the Coulomb friction law gives large but finite fiber axial stresses at the crack tip (Schwietert and Steif, 1991).

Figure 5 shows the axial stresses within the fiber and matrix along the interface as a function of normalized axial location for constant slip lengths. The axial stresses in the fiber are tensile near the crack plane ($z = 0$) and then become compressive for higher z/a values, approaching the value of the remote axial stresses. The matrix axial stresses start at

†An approximate shear-lag analysis using fictitious coefficient of friction.

‡$z = 0$ cannot be chosen as a collocation point because the integrals in the numerical scheme diverge for such cases.

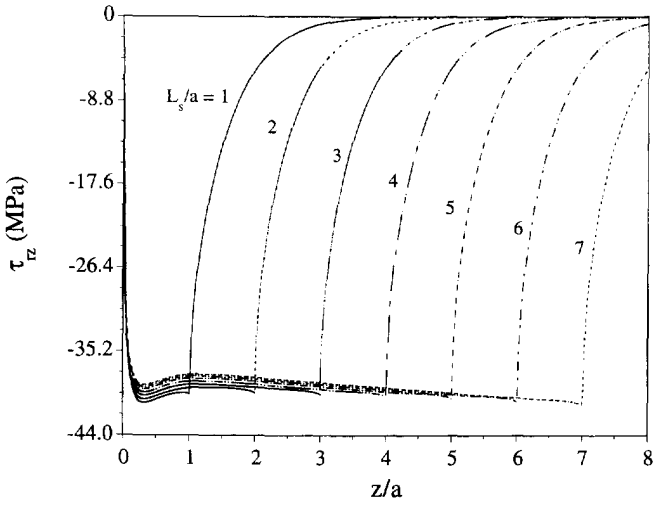

Fig. 4. Boundary layer effect for interfacial shear stress as a function of normalized axial location.

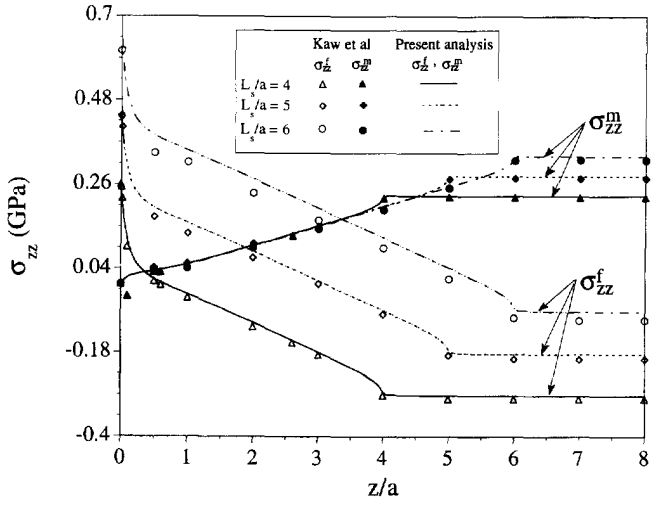

Fig. 5. Interfacial axial stresses as a function of normalized axial location for constant slip lengths.

zero in the crack plane and approach the value of the remote axial stresses at the end of the slip zone. To gain a better insight into the stress values close to the crack plane, we have listed some axial stresses from our present analysis in Table 1 (for $L_s/a = 4$). The comparison between the results from the present analysis and the numerical solution (Kaw *et al.*, 1995) for σ_{zz} is found reasonable in the fiber for all values of z/a and in the matrix away from the crack plane. At points very close the crack plane, the numerical solution of

Table 1. Variation of axial and hoop stresses at the interface with normalized axial location for $L_s/a = 4$

z/a	σ^f_{zz} (GPa)	σ^m_{zz} (GPa)	$\sigma^f_{\theta\theta}$ (GPa)	$\sigma^m_{\theta\theta}$ (GPa)
0	0.27478	0	0.00324	0.24900
0.01	0.25178	0.00205	−0.03020	0.24180
0.02	0.22264	0.00339	−0.04425	0.23664
0.1	0.11385	0.01651	−0.08725	0.22740
0.6	0.00446	0.03769	−0.12552	0.22632

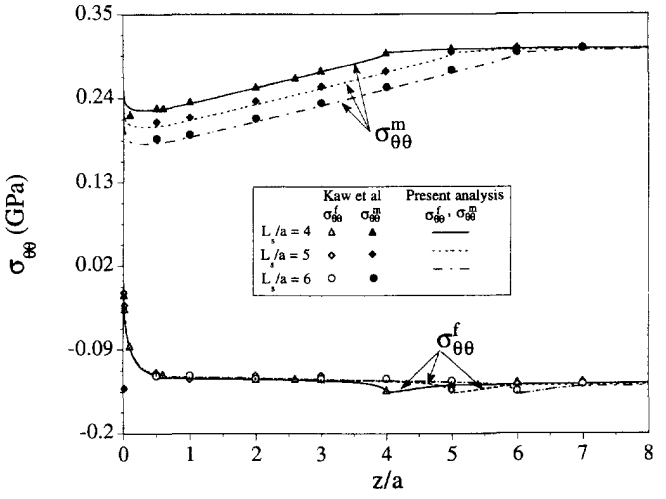

Fig. 6. Interfacial hoop stresses as a function of normalized axial location for constant slip lengths.

Kaw (1995) gives large† negative values of the matrix axial stress. Since in the problem under consideration, no elastic singularities exist, this behavior is unexpected. In contrast, the present solution gives stress values which gradually decay to zero as one approaches the crack plane ($z = 0$) on the matrix side of the interface. Similar observations have been made for other values of slip lengths.

In Fig. 6, we have shown the behavior of the hoop stresses along the interface as a function of the normalized axial location, z/a, for constant slip lengths. The hoop stresses in the fiber are found to be compressive and almost insensitive to the variation of slip length. The hoop stresses in the matrix are tensile and increase away from the transverse crack plane, approaching the value of the remote hoop stress. In Table 1, we have also listed some hoop stresses from the present analysis (for $L_s/a = 4$) to get a clearer picture close to the crack plane. Like axial stress, the hoop stress in the two solutions in the fiber side of the interface agrees reasonably for all z/a values and in the matrix away from the crack plane. At points very close to the crack plane, the numerical solution of Kaw (1995) is again seen to give unexpected large† negative values of the matrix hoop stress. The present solution, on the other hand, gives stress values which gradually approach the hoop stress value at the free surface, $z = 0$.

In Fig. 7, the axial stresses in the fiber and matrix are plotted as a function of the normalized radial location for $L_s/a = 4$. As noted by Kaw *et al.* (1995), the axial stress in the fiber and matrix region are not constant at $z/a = 4$, which is the slip-stick transition length. Both fiber and matrix axial stresses are, however, seen to become nearly independent of the radial coordinate away from the crack plane and the slip-stick transition zone (e.g., at $z/a = 6$). Therefore the assumption of radially independent axial stresses made by Gu and Mangonon (1992) is seen to be valid away from the crack plane and the slip-stick transition zone.

In Fig. 8, we have plotted the normalized crack opening displacement (COD) profiles as a function of the normalized radial location in the matrix, r/a, for constant slip lengths. These profiles are rather flat with the values changing very little across the matrix region. Again, away from the fiber-matrix interface, the comparison between the two solutions is seen to be reasonable. However, at points approaching the fiber-matrix interface, there is a difficulty in computing the COD values from the numerical solution (Kaw, 1995). Finally, in Fig. 9, we have plotted the relative slip ($\Delta w = w^m - w^f$) normalized by the fiber radius, at the fiber matrix interface, as a function of normalized axial location for several values of slip lengths. For points away from the matrix crack plane, we once again observe very good agreement between the two solutions while values at the crack plane ($z/a = 0$) are

†The large stress values arise from the inability to use IMSL (1987) routines for the collocation points close to $z = 0$ in the solution of integral equations. This is because of two reasons: slow convergence of the integrals and possibility of large round-off errors.

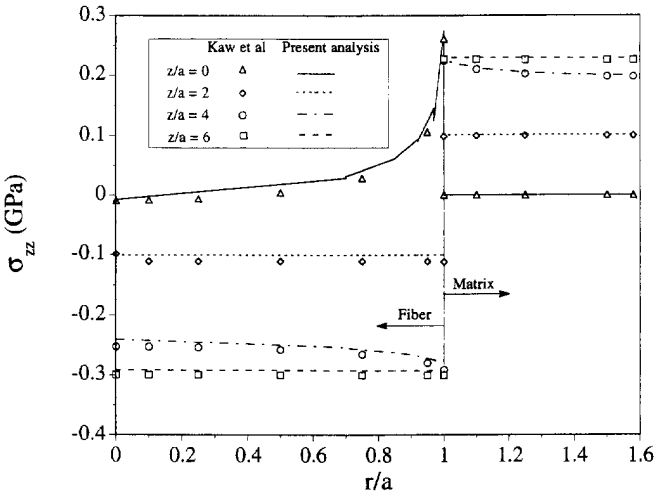

Fig. 7. Fiber and matrix axial stresses as a function of normalized radial location for constant normalized axial location.

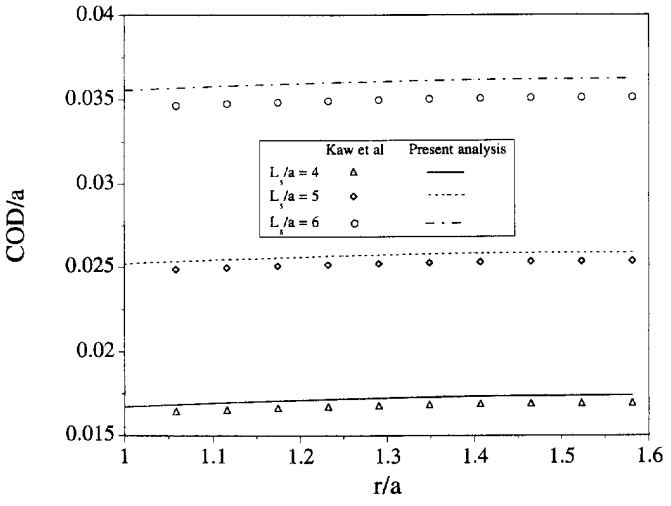

Fig. 8. Normalized crack opening displacement as a function of normalized radial location for constant slip lengths.

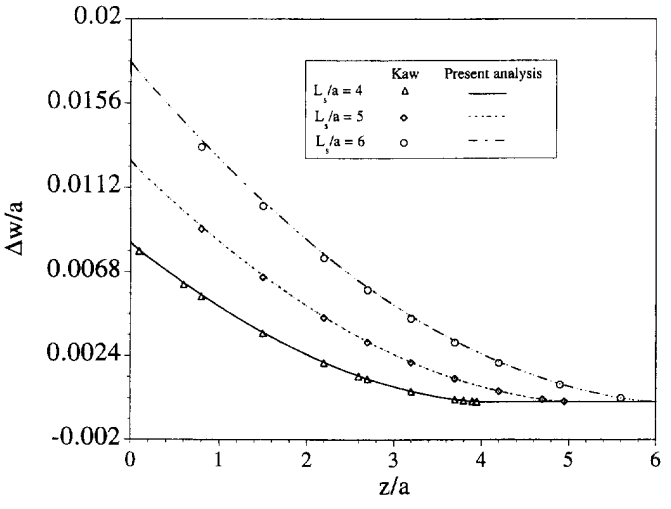

Fig. 9. Normalized relative slip at the fiber-matrix interface as a function of normalized axial location for constant slip lengths.

unavailable due to numerical difficulties (Kaw, 1995). Using a constant shear stress model, Wijeyewickrema and Keer (1993) noted that the maximum slip occurs away from the crack plane and that the peak decreased with increasing slip length. Unlike their stated observation, the maximum slip is seen to occur at the crack plane for all values of slip lengths investigated in this work and is seen to increase with increasing values of L_s/a. The increase in slip (Δw) is consistent with increase in the applied value of remote displacement needed to give rise to larger slip lengths.

CONCLUDING REMARKS

The objective of this work was to examine the stresses and displacements in the vicinity of a bridged matrix crack touching a frictionally constrained interface and to establish the accuracy of the variational model employed by comparing it to existing elasticity solutions. The stress field for the stated problem is found to be bounded for the class of materials considered in this study. Unlike other solutions reported in the literature which satisfy boundary conditions in a limited sense, the present approach is seen to satisfy all boundary and inequality conditions in the slip and stick regions and at the slip-stick transition point. The results of the present analysis are shown to be in very good agreement with the numerical elasticity solution of Kaw *et al.* (1995) for points away from the matrix crack tip (located at the fiber-matrix interface). At or very near the crack plane ($z = 0$), the numerical solution of Kaw (1995) is seen to give rather unexpected results in the behavior of matrix axial and hoop stresses, while there are numerical difficulties in evaluating crack opening displacement and axial slip at the crack tip.

In this study, we have also demonstrated the existence of a boundary layer effect for the behavior of the radial and shear stresses in the slip region. Various approximate models available in the literature, which assume a constant value of shear stress in the slip region, therefore neglect the boundary layer effect observed in this study. The radial stress is found to be compressive over the entire length of the continuous zone, even though this was not enforced as an additional requirement, for the problems analyzed in this work. The axial stresses in the fiber and matrix region are shown to become nearly independent of the radial coordinate away from the crack plane and the slip-stick transition zone. Further, the Coulomb friction law employed in this study gives large but finite fiber axial stresses at the crack tip, whereas, a constant shear stress assumption gives logarithmically singular fiber axial stresses at the crack tip. Unlike the observation of Wijeyewickrema and Keer (1993), maximum slip (Δw) is seen to occur at the crack plane for all values of slip lengths investigated and is seen to increase with increasing values of L_s/a. The slip length itself is seen to increase monotonically with an increase in stress ratio (negative of remote matrix axial stress to remote interfacial radial stress) and decreases with an increase in coefficient of friction. As shown by Kaw *et al.* (1995), the results of elasticity analysis converge to approximate shear-lag analysis results only for large values of slip lengths.

Finally, in the example treated, we have solved the inverse problem, i.e., for a given value of the slip length (and assuming no opening), we have calculated the applied value of the remote displacement needed to give rise to the assumed value of slip length. We have assumed that there is continuity of radial stress and displacement along the entire interface. In practice, this may not be the case. The direct problem to consider is that of a matrix crack impinging on an interface while the composite is loaded incrementally up to a specified level. Is it now possible to postulate a logical sequence of failure events corresponding to the applied load level? As shown by McCartney (1989) and Pagano and Brown (1993), the radial interface stress reverses to tension (assuming perfect bonding and $\alpha_m > \alpha_f$) in the presence of an annular matrix crack, setting up the possibility of debonding under small tensile loads applied to the composite. We could then have an open zone along the fiber-matrix interface ahead of the matrix crack tip. This problem which would then involve calculating the lengths of both the open and slip zones is certainly much more complex. The equations governing the solution of this problem have already been presented in this study. Our current effort is directed towards devising a methodology to obtain the solution

to the posed problem, which has not been addressed (perhaps even not discussed) in the literature.

Acknowledgements—The authors would like to thank Dr Autar K. Kaw, University of South Florida, Tampa, for extensive discussions and for providing comparative numerical results.

REFERENCES

Aveston, J., Cooper, G. A. and Kelly, A. (1971). Single and multiple fracture. In *The Properties of Fibre Composites, Conference Proceedings, National Physical Laboratory*, pp. 15–26. IPC Science and Technology Press Ltd, Guildford, UK.

Brown III, H. W. (1992). Analysis of axisymmetric micromechanical concentric cylinder model. In *Seventeenth Annual Mechanics of Composites Review, Air Force* 86145/09-10-92-150, Dayton, OH, U.S.A.

Budiansky, B., Hutchinson, J. W. and Evans, A. G. (1986). Matrix fracture in fiber-reinforced ceramics. *J. Mech. Phys. Solids* **34,** 167–189.

Chawla, K. K. (1987). *Composite Materials*, Springer-Verlag, New York, NY, U.S.A.

Dollar, A. and Steif, P. S. (1988). Load transfer in composites with a Coulomb friction interface. *Int. J. Solids Structures* **24,** 789–803.

Dollar, A. and Steif, P. S. (1989). A tension crack impinging upon frictional interfaces. *ASME J. Appl. Mech.* **56,** 291–298.

Gu, L. and Mangonon, P. L. (1992). Mechanical characteristics of fiber-reinforced brittle matrix composite. Case II: Non-zero radial stress at matrix external surface. In *Constitutive Behavior of High-Temperature Composites* (MD-Vol 40), pp. 151–161. American Society of Mechanical Engineers, New York, NY, U.S.A.

Hseuh, C. and Becher, P. F. (1988). Thermal expansion coefficients of unidirectional fiber-reinforced ceramics. *J. Am. Ceram. Soc.* **71,** C438–C441.

Hseuh, C. and Becher, P. F. (1989). Correction to thermal expansion coefficients lof unidirectional fiber-reinforced ceramics. *J. Am. Ceram. Soc.* **72,** 359.

IMSL (1987). *IMSL FORTRAN Subroutines for Mathematical Applications, Math/Library, Version* 1.0. IMSL, Dallas, Texas, U.S.A.

Kaw, A. K. and Pagano, N. J. (1993). Axisymmetric thermoelastic response of a composite cylinder containing an annular matrix crack. *J. Comp. Mater.* **27,** 540–571.

Kaw, A. K. (1995), personal communication.

Kaw, A. K., Kunchithapatham, S. and Pagano, N. J. (1995). Stress field in a cracked brittle matrix composite cyclinder with a frictional interface. *Int. J. Solids Structures* **32,** 2127–2154.

Kelly, A. (1970). Interface effects and the work of fracture of a fibrous composite. *Proc. R. Soc. London* **A319,** 95–116.

McCartney, L. N. (1989). New theoretical model of stress transfer between fibre and matrix in a uniaxially fibre-reinforced composite. *Proc. R. Soc. London* **A425,** 215–244.

Meda, G., Hoysan, S. F. and Steif, P. S. (1993). The effect of fiber Poisson expansion in micro-indentation tests. *ASME J. Appl. Mech.* **60,** 986–991.

Pagano, N. J. (1991). Axisymmetric micromechanical stress fields in composites. *Proceedings* 1991 *IUTAM Symposium on Local Mechanics Concepts for Composite Materials Systems*, p. 1. Springer Verlag, Berlin.

Pagano, N. J. and Brown III, H. W. (1993). The full-cell cracking mode in unidirectional brittle-matrix composites. *Composites* **24,** 69–83.

Reissner, E. (1950). On a variational theorem in elasticity. *J. Math. Physics* **29,** 90.

Schwietert, H. R. and Steif, P. S. (1991). An integral equation method applied to a crack impinging upon a bimaterial frictional interface. *Int. J. Fract.* **49,** 257–272.

Selvadurai, A. P. S. (1994). Matrix crack extension at a frictionally constrained fiber. *J. Engng Mater. Tech.* **116,** 398–402.

Steif, P. (1984). Stiffness reduction due to fiber breakage. *J. Comp. Mat.* **17,** 153–172.

Wang, Y. C., Hui, C. Y., Lagoudas, D. and Papadopoulos, J. (1991). Small-scale crack blunting at a bimaterial interface with Coulomb friction. *Int. J. Fract.* **52,** 293–306.

Wijeyewickrema, A. C. and Keer, L. M. (1993). Matrix cracking in a fiber reinforced composite with slip at the fiber-matrix interface. *Int. J. Solids Structures* **30,** 91–113.

APPENDIX

$$\eta_{11} = \frac{r_2 w^{*\prime} - \hat{w}'}{r_2 - r_1} \quad \eta_{12} = \frac{\hat{w}' - r_1 w^{*\prime}}{r_2 - r_1}$$

$$\eta_{21} = \frac{r_2 \bar{u} - u^*}{r_2 - r_1} \quad \eta_{22} = \frac{u^* - r_1 \bar{u}}{r_2 - r_1}$$

$$\eta_{31} = \frac{2u^* - r_2 \bar{u}}{r_2 - r_1} \quad \eta_{32} = \frac{r_1 \bar{u} - 2u^*}{r_2 - r_1}$$

$$\eta_{33} = -r_1 r_2 (r_1 + r_2)\bar{u} + 2(r_1^2 + r_1 r_2 + r_2^2)u^* - 4\bar{u}$$

$$\eta_{34} = -r_1 r_2 \bar{u} + 2(r_1 + r_2)u^* - 3\hat{u}$$

$$\eta_{35} = \begin{cases} \dfrac{(r_1 + r_2)\bar{u} - 2u^*}{r_1 r_2} & \text{if } r_1 \neq 0 \\ 0 & \text{if } r_1 = 0 \end{cases}$$

$$\eta_{51} = \begin{cases} \dfrac{3\hat{w} - 2r_2 w^* + r_2 \hat{u}' - \bar{\bar{u}}'}{r_1(r_2 - r_1)} & \text{if } r_1 \neq 0 \\ 0 & \text{if } r_1 = 0 \end{cases}$$

$$\eta_{52} = \begin{cases} \dfrac{2r_1 w^* - 3\hat{w} + \bar{\bar{u}}' - r_1 \hat{u}'}{r_2(r_2 - r_1)} & \text{if } r_1 \neq 0 \\ \dfrac{\hat{u}' - 2w^*}{r_2} & \text{if } r_1 = 0 \end{cases}$$

$$\eta_{53} = \begin{cases} \dfrac{(r_1^2 + r_1 r_2 + r_2^2)(2w^* - \hat{u}') + (r_1 + r_2)(\bar{u}' - 3\hat{w}) + r_1^2 r_2^2 \bar{u}'}{r_1^2 r_2^2} & \text{if } r_1 \neq 0 \\ 2r_2 w^* - 3\hat{w} + \bar{\bar{u}}' - r_2 \hat{u}' & \text{if } r_1 = 0 \end{cases}$$

with

$$\eta_{iJ} = 0 \quad (i = 1, 2 \text{ and } J = 3, 4, 5 \text{ or } i = 5 \text{ and } J = 4, 5).$$